

# Hundreds of new periodic signals detected in the first year of *TESS* with the *weirddetector*

Joheen Chakraborty<sup>1\*</sup>, Adam Wheeler<sup>1</sup> and David Kipping<sup>1,2</sup>

<sup>1</sup>*Dept. of Astronomy, Columbia University, 550 W 120th Street, New York NY 10027*

<sup>2</sup>*Flatiron Institute, 162 5th Av., New York, NY 10010*

Accepted . Received ; in original form

## ABSTRACT

We apply the *weirddetector*, a nonparametric signal detection algorithm based on phase dispersion minimization, in a search for low duty-cycle periodic signals in the Transiting Exoplanet Survey Satellite (*TESS*) photometry. Our approach, in contrast to commonly used model-based approaches specifically for flagging transits, eclipsing binaries, or other similarly periodic events, makes minimal assumptions about the shape of a periodic signal, with the goal of finding “weird” signals of unexpected or arbitrary shape. In total, 248,301 *TESS* sources from the first-year Southern sky survey are run through the *weirddetector*, of which we manually inspect the top 21,500 for periodicity. To minimize false-positives, we here only report on the upper decile in terms of signal score, a sample for which we obtain 97% recall of *TESS* eclipsing binaries and 62% of the TOIs. In our sample, we find 377 previously unreported periodic signals, for which we make a first-pass assignment that 26 are ultra-short periods ( $< 0.3$  d), 313 are likely eclipsing binaries, 28 appear planet-like, and 10 are miscellaneous signals.

**Key words:** eclipses — planets and satellites: detection — methods: numerical — stars: planetary systems

## 1 INTRODUCTION

With the recently-launched Transiting Exoplanet Survey Satellite (*TESS*; Ricker et al. 2015) observing on the order of  $10^6$  unique targets across the full sky and boasting an anticipated yield of thousands of novel exoplanets (Sullivan et al. 2015, 2017; Bouma et al. 2017; Barclay et al. 2018; Ballard 2019), there is a need for varying approaches to the analysis of *TESS* data products to make full use of the survey’s wide scope and potential. The large survey size and all-sky nature of *TESS* make it particularly adept for catching uncommon signals, of potentially ill-classified or even unknown shape. These “needles in the haystack” may challenge our understanding of other stars and spark new theoretical developments, such as the case of Boyajian’s Star (Boyajian et al. 2016; Wright et al. 2016; Bodman & Quillen 2016; Foukal 2017; Katz 2017; Neslusan & Budaj 2017; Ballesteros et al. 2018; Wyatt et al. 2018; Martinez et al. 2019; Sucerquia et al. 2019). Accordingly, new methods to flag these signals for closer inspection have been developed in recent years to expedite their recovery (Giles & Walkowicz 2019; Schmidt 2019; Wheeler & Kipping 2019).

The development of these new methods also serves to

benefit the recovery of more conventional signals that may have been missed by more standard approaches, such as Box Least Squares (Kovács et al. 2002, 2006). For example, many of the known *Kepler* single- and double- transiting systems come from a myriad of independently developed search methods (Schmitt 2017; Uehara et al. 2016; Wang et al. 2015; Foreman-Mackey et al. 2016; Kawahara & Masuda 2019), including one specifically designed to find unusual signals (Wheeler & Kipping 2019).

The latter approach, known as the *weirddetector*, was previously successfully run on the 161,786 *Kepler* sources, where it identified the 6 aforementioned missed mono/stereo transits, but also another 18 previously missed periodic signals consistent with binary star systems. Given the similarities between the *Kepler* and *TESS* data products, this makes the *weirddetector* attractive as an automated search tool for *TESS* too. The *weirddetector* is a signal detection algorithm with the goal of relaxing assumptions about signal shape in order to detect events of abnormal morphology (Wheeler & Kipping 2019). Whilst the *weirddetector* is not specifically intended for exoplanet transit detection, it is related to the more planet-specific search methods, in that it accounts for a different set of potential signals. Accordingly, the *weirddetector* is able to detect a wider variety of signals than just, say, transiting planets or eclipsing binaries

\* E-mail: [jc5110@columbia.edu](mailto:jc5110@columbia.edu)

(though it is also able to recover to those events), at the cost of lower sensitivity to signals of *a-priori* known shape.

In this work, we apply the **weirddetector** to 248,301 target light curves from sectors 1 through 13, which represents *TESS*'s first-year survey of the Southern sky. From these, we manually identify 468 significant periodic signals which appear to not have been previously reported, with particular attention given to the top 30 of these. In Section 2, we briefly describe the algorithm and the specific changes made for *TESS*. In Section 3, we discuss the application of the code, cross-reference the findings with those of other catalogues, and introduce the most likely signals detected which are previously undetected at the time of writing. In Section 4, we discuss further improvements and potential continuations of our work.

## 2 METHODOLOGY

The basic principle of the **weirddetector** is to identify high-likelihood periodic signals for manual inspection while abandoning any parametric function to describe the transit shape. We emphasize that the **weirddetector** algorithm cannot identify signals all on its own, but instead facilitates a subsequent informed manual search through the high-probability signals sorted by the algorithm; as such, it is most useful to consider usage of the **weirddetector** algorithm as one part in a larger search pipeline. A more in-depth discussion of the **weirddetector** is available in [Wheeler & Kipping \(2019\)](#), but we shall also include a brief description, highlighting in particular the points specific to our application on *TESS* data.

### 2.1 General principles of weirddetector

As the **weirddetector** searches for coherent, low duty-cycle periodic signals, the algorithm folds on many trial periods and searches for the period values which exhibit the smallest dispersion of fluxes. We note that phase dispersion minimization is not a novel concept—it has been used in other algorithms such as the Plavchan periodogram ([Plavchan et al. 2008](#); [Parks et al. 2014](#)). In the case of *TESS*, which monitors each field for  $\simeq 27$  days, we opt for a period grid ranging from 0.25 days up to 15 days uniform in  $\log P$  (24,567 total period values). Just as was found with *Kepler* though ([Wheeler & Kipping 2019](#)), the algorithm is sensitive to periods outside the period grid if there is a harmonic of the true period within the grid (which is the case for some of our flagged signals later).

To quantify the relative success at phase dispersion minimization of a given trial period, the **weirddetector** examines the chi-squared ( $\chi^2$ , which reflects how scattered the values are) and kurtosis ( $\kappa$ , which reflects the weight of a distribution's tail relative to its peak). The algorithm then calculates *excess* kurtosis,  $\kappa' = \kappa - \kappa_{\text{Gaussian}}$  and chi-squared less than the median,  $\Delta\chi^2 = \text{median}(\chi^2) - \chi^2_{\text{period}}$ . These two metrics are multiplied to form a score strength, such that we require both perform well to yield a putative signal. To normalize the scores, we re-calculate  $\kappa'(P)\Delta\chi^2(P)$  along a grid of periods but for a scrambled version of the original data (which should have no periodicity), and evaluate a sliding

standard deviation of the result,  $\sigma(P)$ . Using these quantities, the algorithm defines a final merit function,  $\zeta$ , for each period value, given by  $\zeta(P) = \kappa'(P)\Delta\chi^2(P)/\sigma(P)$ .

The above value of the merit function gives us intuition about the ideal signal the **weirddetector** is searching for. To maximize the merit function of a period  $P_{\text{ideal}}$ , the phase curve should be much more coherent at  $P_{\text{ideal}}$  than at other “random” values of  $P$  (i.e. large decrease in  $\chi^2$ ); the phase curve should hover around a constant value with only one (or a few) short excursion(s) from the baseline (i.e. high excess kurtosis  $\kappa'$ ); and these two conditions should otherwise have low variation at nearby  $P$ -values not equal to  $P_{\text{ideal}}$ , maintaining small values for  $\Delta\chi^2$  and  $\kappa'$  to demonstrate there is, in fact, a distinct signal with a specific period more likely than the rest (i.e. low  $\sigma(P)$ ).

### 2.2 Differences between Kepler and TESS

The **weirddetector** is highly versatile and generalizable, and was able to run on *TESS* data after appropriate changes were made from the implementation for *Kepler*. Following are the details that are sensitive to the particular telescope gathering the data.

*Kepler* observed a 115 square-degree patch of sky, at a cadence of 30 minutes for 17 quarters of up to 90 days each. *TESS*, on the other hand, generates light curves with a cadence of 2 minutes and will observe 26 different sectors for  $\simeq 27$  days each. *TESS*, while it spends only a month on the targets of each sector (barring targets that receive extra coverage as a result of overlap between sectors), will survey 85% of the sky, covering roughly 400 times as many unique stars as *Kepler*. As a result, there will be far more data to search through; however, by virtue of the shorter baseline, we are more limited in the range of periods for which we can detect signals.

In addition, having fewer data points means the **weird-detector** will be more sensitive to outlier events when calculating both  $\chi^2$  and  $\kappa$ , such as stellar flares or instrument-caused deviations. As a result, we were more stringent in our outlier rejection when considering the phase-folding part of the algorithm to limit one-time events from inducing spurious signal detections or leading to false positives by unfavorably skewing  $\kappa$ . Additionally, while we do not expect  $\kappa$  or  $\sigma$  to change much,  $\chi^2$  (and therefore  $\Delta\chi^2$ ) is orders of magnitude lower in *TESS* because of the fewer points in the light curves. This means that  $\zeta$  drops accordingly; however, because the *absolute* values of  $\zeta$  do not matter as much as the *relative* values for determining the most promising period values, and we take the step of dividing by  $\sigma(P)$ , our analysis is little-affected.

We also had to adjust the bandwidth used for our median-filter detrending algorithm to better reflect the duration of the signals we were searching for while considering the shorter range of trial periods we were folding on. In addition, the presence of *TESS*'s regular data gaps posed an issue, as *Kepler* data suffered far fewer gaps per unit time. However, as these changes did not require fundamentally altering the algorithm, their treatment is discussed in the beginning of Section 3.

### 2.3 Aliases

One major limitation of the **weirddetector** is its tendency to flag rational fractions or multiples (“aliases”) of the true period of a signal. This is unavoidable when using a folding technique with such relaxed requirements for signal shape, and the issue is not specific to *TESS* light curves.

Here, we partially corrected for this error by attempting to automatically flag the correct period when an integer multiple was identified in the case of single-dip signals. It is important to note that a) our technique *only* accounts for flagged periods that are an integer multiple of the true period (which we chose to target because it is the most common case of aliasing); and b) we still need to manually examine the data to determine if the period detected is truly the correct one. Still, our technique helps us identify signals by suggesting the correct period more frequently.

For a single-dip event with true period  $P_{\text{true}}$  and flagged period  $P_{\text{flagged}}$ , there will be  $n = (P_{\text{flagged}}/P_{\text{true}}) : n \in \mathbb{Z}^+$  dips in the phase curve folded with  $P_{\text{flagged}}$ . By automatically detecting the number of dips  $n$ , we can therefore retrieve the correct period by multiplying. We identify a dip by the following: examine the points in folded time-order in 200-point sliding windows. If greater than one-third of the points in this window have a flux value that falls under  $1.5\sigma$  below the median, note the window as the beginning of a dip. Then, wait for the flux values to return to normal before looking for another dip by flagging the *end* of a dip when greater than three-quarters of the window has a value within  $\sigma$  of the median (see Figure 1). Note that the specific time picked out by the sliding window is not important, as this approach does not need to consider the duration or shape or the dip—only the *number* of significant dips  $n$ .

The specific numerical values were chosen heuristically to handle the aforementioned case of aliasing—by far the most common case within our data. Though a similar approach may work in principle for regular increases in flux, there are too many confounding factors (particularly flares) to have a reliable solution to that problem.

## 3 APPLICATION TO TESS DATA

### 3.1 Data preparation

We ran the **weirddetector** on all light curve files in sectors 1 through 13 available at [MAST](#) (248,301 not including overlap of targets between sectors; 223,087 unique targets after considering overlap). We remove probable outliers from each PDC light curve by removing points more than  $6 \times \text{MAD}$  away from the median in an 11-point rolling window, where MAD is the median absolute deviation:  $\text{median}(|F_i - \text{median}(F)|)$ . (As one of the key assumptions of **weirddetector** is the presence of Gaussian noise, we can use MAD as an estimator of the standard deviation with  $\sigma = 1.4826 \times \text{MAD}$ , meaning our threshold is also roughly equal to  $4\sigma$ ). We also removed all points with non-zero quality flags in the FITS files.

In each sector, we split each PDC time series into two segments (“semi-sectors”) before and after the  $\sim 1$  day data gap. Within each segment, we used linear interpolation to fill in missing data and detrended with a moving median filter, using a 1 day bandwidth, to remove long-term trends, following (Wheeler & Kipping 2019). We decided on the 1-

day window as it is both sufficiently shorter than the duration of observation (27 days per target) and longer than the duration of our signals of interest (most are of order  $10^{-1}$  days). This also acts to suppress long duty-cycle signals associated with stellar rotation. After detrending, we removed the interpolated points and recombined the segments. The **weirddetector** was then run on the 24,567 trial periods for 248,301 unique light curves.

### 3.2 Filtering

In order to preserve only the most likely signal candidates and remove artifacts of the data analysis, some cuts were made to the resultant data. The first one we note is that upon examining a scatter plot of a light curve’s  $\log \zeta_{\text{peak}}$  versus  $\log P$ , one immediately sees piling up a certain frequencies. A similar effect was reported by Wheeler & Kipping (2019) on the *Kepler* data. These are immediately suspicious as spurious common modes, rather than astrophysical signals. We therefore proceeded to design a means to filter out these suspicious periods.

Since the distribution of periods guessed by the **weirddetector** was at first not log-uniform (in particular with large saturation towards the upper end), we cut the 1,000 most commonly appearing periods to achieve a more uniform distribution (Figures 2b-c). Though the precise number chosen as a cutoff was somewhat ad-hoc, it accomplished the desired goal of picking out a set of signals with a more uniform distribution of  $\log(P)$ .

Even after cuts, there are a few peculiarities in the distribution worth addressing. There is a low density of points at  $\log(P) \approx 0.8$ ; we posit these are caused by phasing of periods which are almost exactly half ( $\approx 6.5$ ) of the 13-day semi-sector baseline, causing dips to frequently fall within the one-day gap. We also note a concentration of high- $\zeta_{\text{peak}}$  points close to  $\log(P) = -0.3$ ; these could be caused by a common mode, as they are unlikely to be astrophysical considering their distance from the rest of the distribution. The high- $\zeta$  signals are denser at the higher end of  $P$ -values even after cuts, which is likely due to lower  $\chi^2$  values caused by the lesser dispersions associated with folding on longer periods; this trend contributes significantly to the aliasing effect of rational multiples  $P_{\text{true}}$  as noted in Section 2.3

Since our goal is to find new signals, known variables from the Villanova eclipsing binary catalogue (Prsa 2020), the ASAS-SN catalog of variable stars (Shappee 2014; Jayasinghe et al. 2018, 2019), the International Variable Stars Index (VSX, Watson et al. (2006)), and the TESS Objects of Interest (TOIs) (NASA Exoplanet Archive list of current TOIs) were also removed. Altogether, these cuts comprised roughly 13% of the data, leaving 215,871 of the 248,301 targets intact.

We consider a signal to be “interesting” if its periodogram has a most-significant peak such that  $\zeta \geq \zeta_{\text{threshold}}$ , again following Wheeler & Kipping (2019). We choose  $\zeta_{\text{threshold}}$  not independently at some fixed value, but set it to pick out the top decile of candidates, after cutting both common periods and already-discovered signals, for manual inspection. We look only at the most-significant peak (and rational fractions) as found by the previously described method, to generate phase curves with the highest likelihood of containing the correct period.

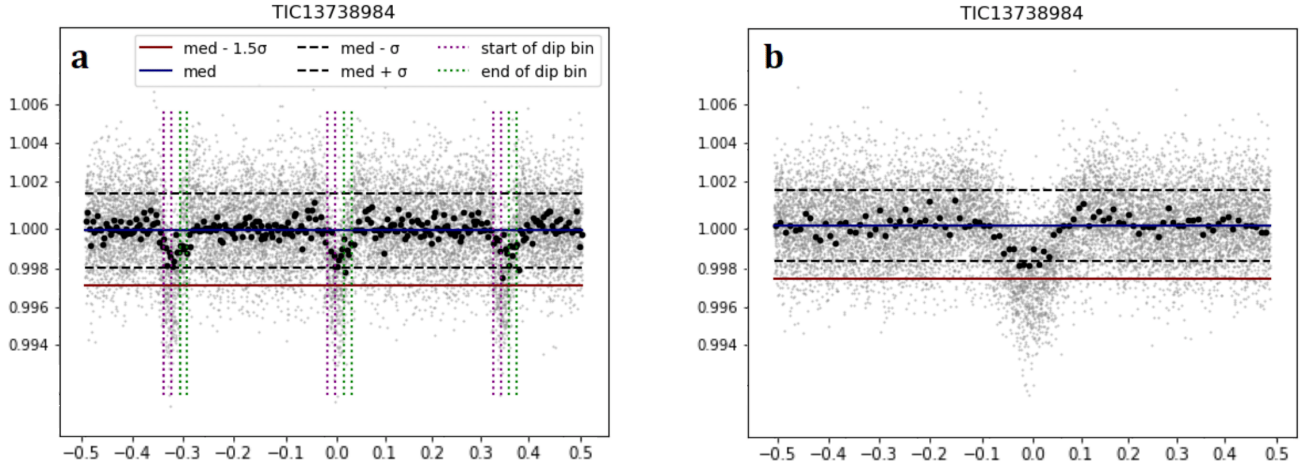


**Figure 1.** a: A sample flagged signal (TIC 13738984) with  $\zeta_{\text{peak}}$  at a  $P_{\text{flagged}}$  which is an integer multiple of  $P_{\text{true}}$ . Here,  $\frac{P_{\text{flagged}}}{P_{\text{true}}} = 3$ . The solid blue line indicates  $\text{median}(F)$ ; the solid maroon line indicates  $\text{median}(F) - 1.5\sigma$ , the threshold below which we take the beginning of a dip; and the dashed gray lines indicate  $\text{median}(F) \pm \sigma$ , the range at which we take the end of a dip. The vertical lines indicate the boundaries of the 200-point bins which mark the starts and ends of the dips. b: The result of using the algorithm, which successfully picks out the correct period.

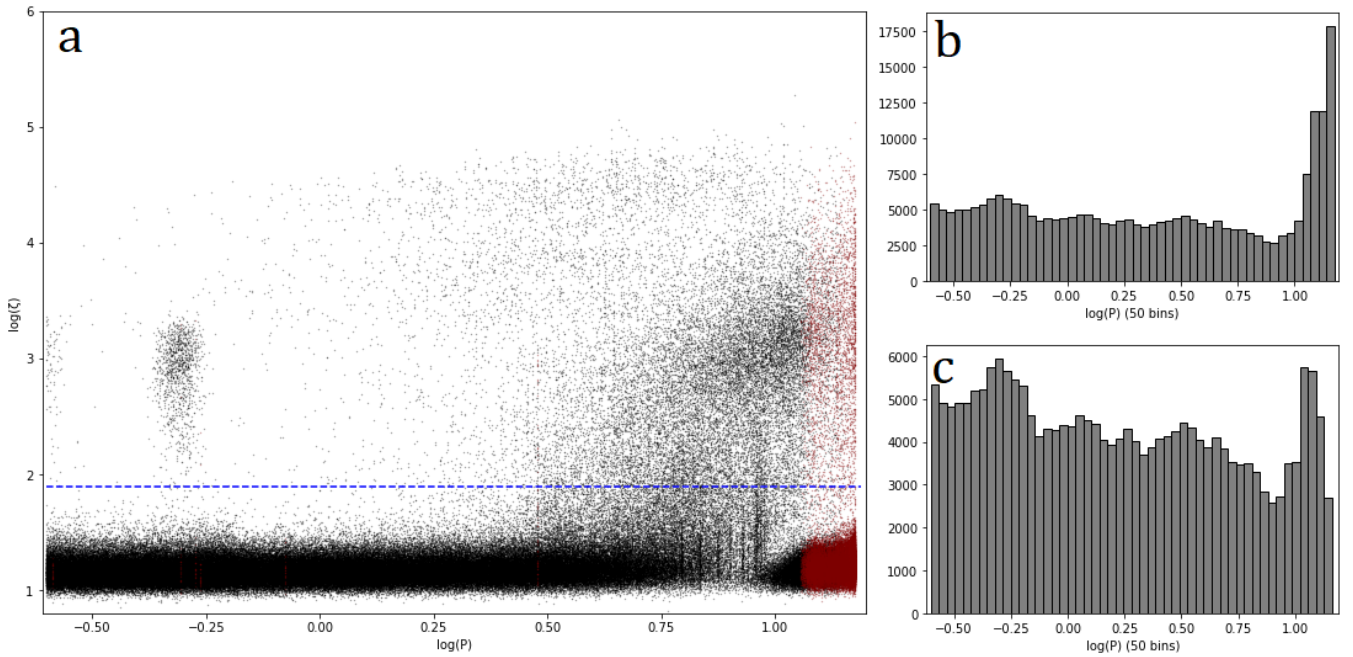


**Figure 2.** a: Flagged period values with cut (over-represented) periods marked in red. The blue line represents  $\zeta_{\text{threshold}}$ , the cutoff for  $\log_{10}(\zeta_{\text{peak}})$  above which we manually inspected for signals. b: Histogram of  $\log_{10}(P)$  before cutting over-represented period values (50 bins). There is significant saturation towards the tail end, as represented in Fig. 2a. c: Histogram of  $\log_{10}(P)$  after cutting over-represented periods (50 bins). This graph is more evenly distributed, as desired.

### 3.3 Data products

After filtering, we flag 377 previously-unidentified targets (dubbed Weird Objects of Interest, or WOIs) that appear to contain some periodic signal. The signals were selected manually based on whether their phase curves showed a clear signal (or multiple clear signals, in the case of aliases).  $\zeta_{\text{peak}}$  values of the WOIs fall within the range of  $10^3$  to  $10^5$ , pro-

viding evidence that the selected periods are several orders of magnitude better than naive guessing. Additionally, we examined distributions of  $\Delta\chi^2$  and  $\kappa$  for the WOIs, which showed no dependence on each other, assuring us that the high  $\zeta_{\text{peak}}$  values are not artifacts. In Table 1, we present the  $\zeta_{\text{peak}}$  and periods, along with accompanying information, for the WOI signals reported in this work.

To ensure each signal was not an artifact of the median-



filter detrending, we applied different detrending algorithms to the raw light curves and re-folded on the flagged period. We applied the implementation of Cosine Filtering with Autocorrelation Minimization (CoFiAM; Kipping et al. 2013) found in the MoonPy Python library, as well as phasma, a non-parametric phase-folding algorithm (Jansen & Kipping 2018). Example phase curves presented in Figures 3 & 4 have been detrended with phasma. We also queried the TIC-8 catalog (Stassun et al. 2018) for these objects to report their basic stellar properties, which is provided in the figure panels where available. We provide moving median, CoFiAM and phasma detrended phase curves for the 337 signals, as well as a CSV form of Table 1 at [this URL](#).

### 3.4 Performance

To quantify the **weirddetector**’s performance, we analyzed its effectiveness at recovering signals from the Villanova eclipsing binary and TOI catalogues. At the time of writing, 62% of currently-documented TOIs (1267/2044) and 97% (1801/1855) of Villanova eclipsing binaries fell within the top decile of  $\zeta_{\text{peak}}$  values. The missing targets in each catalog are expected, as ideally a model-based approach would be best for finding transiting planets and eclipsing binaries, respectively, whereas the **weirddetector** is sensitive to all manner of periodic signals. We note also that all of the missing targets from the Villanova EB catalogue have periods falling outside our period grid ( $> 15$  days), explaining the algorithm’s failure to recover them. We maintained a high recall (the fraction of catalogued true signals recovered) percentage at the cost of precision (the fraction of flagged signals which we know or believe are real), as we wanted to minimize false negatives over false positives to find as many interesting signals as possible. Of course, one could vary the fraction of signals we consider from 10% to modify the precision and recall percentages (Figure 5).

## 4 DISCUSSION

In this work, we have applied the **weirddetector** designed to flag high-likelihood periodic signals of arbitrary shape in time series photometry for subsequent manual inspection, to 248,301 unique TESS targets in Sectors 1-13 (the year-one Southern sky survey). Full frame image targets were not analyzed. Our work identifies 377 very high signal to noise periodic signals that have not been previously flagged in the literature or elsewhere to our knowledge. We have provided basic parameters and identifiers for these systems to enable community follow-up. The number of WOIs could surely be increased by relaxing our threshold to consider more than the top decile of  $\zeta_{\text{peak}}$  events. This choice was made to allow us to quickly hone in on the most significant signals - the goal is to perform triage here and simply see if there is something glaringly obvious and exciting in the TESS data. Having done so, we can report that amongst the 377 WOIs identified, none of them appear to display the kind of remarkably unusual behaviour observed for Boyajian’s Star (Boyajian et al. 2016), despite the fact the **weirddetector**

easily recovered that signal in the *Kepler* timeseries<sup>1</sup>. This does not mean analogs do not exist amongst the target stars. While the new signals uncovered in this survey suggest gaps in the completeness functions of other detection methods, it remains unclear exactly what these gaps are. One could go about precisely identifying them with a detailed injection and recovery hare-and-hound exercise across several different search strategies, but that is beyond the scope of this work. By the same token, we cannot directly convert our lack of detection into an occurrence rate of Boyajian-like stars (nor is it immediately clear how one would define such events).

We also highlight that it is not the objective of this work to offer astrophysical interpretations of the identified signals. They are simply flagged periodic signals that have been apparently missed thus far, in the same vein as the *Kepler* study by Wheeler & Kipping (2019). Nevertheless, we will offer some simple classifications below.

We highlight that the periods in Table 1 are only estimates and it is possible the true period is an alias. Still, in many cases we find extremely short flagged periods, less than 0.3 days, which we classify as “ultra short period” (USP). If correct, these are unlikely to be eclipses since for a Solar-like host the orbital period would be grazing or inside the star. A possible explanation is a rapidly rotating star, which could be checked with a  $v \sin i$  measurement, or pulsations - which might be expected in the case of evolved stars with lower  $\log g$  values. As an example, TIC 443494351 is a USP but also has an excessively long duty cycle for its “dip” (which is itself questionable in nature). This makes it unlikely to be an eclipse signal and more consistent with intrinsic stellar activity. We classify 26 of the cases as USPs.

The overwhelming majority of WOIs appear to be eclipsing binary systems, as evident from inspection of Figures 3 & 4. We can crudely classify an “EB” as one which displays a) two dips per period, or b) one dip and noticeable phase curve variations, or c) one dip with a depth greater than 2%. Using this criterion, and excluding the ultra short periods mentioned above, we classify 313 of the WOIs as likely EBs.

A third classification we offer is “planet-like” (PL). These are signals which appear consistent with a transiting planet from the phase curve morphology alone, but have not been subject to any further vetting. We classify signals as planet-like if they show no noticeable phase curve variations and have one-dip per period which is less than 2% in depth. We also impose the condition that the duration of the dip must be less than one-sixth of the orbital period (which corresponds to a planet with  $a/R_\star > 2$ ). This results in 28 planet-like signals. This leaves 10 WOIs without a clear classification - within which we suspect stellar activity may be broadly responsible.

Amongst the WOIs, there are some curious signals, such as TIC 24347173. A 2% phase curve appears consistent with rotational modulation giving the phasing with respect to the dips, yet the strict coherence implies an apparent 2:1

<sup>1</sup> Note that Boyajian’s Star is not strictly periodic, but like the detection of mono-transits by the **weirddetector**, the kurtosis aspect of its merit function provides sensitivity to even one-off events - although it is certainly not optimized to them.

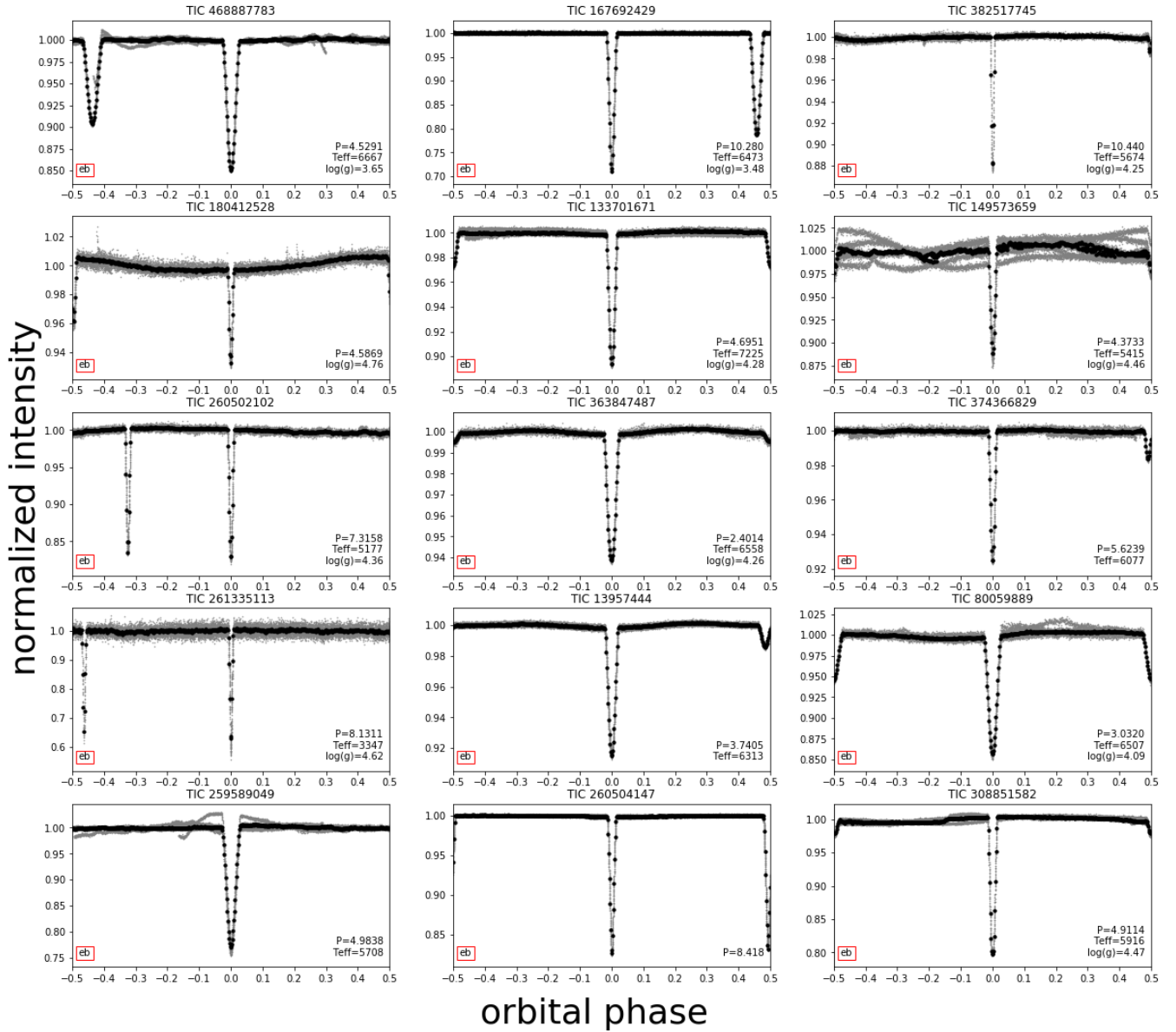


**Figure 3.** The first to fifteenth highest scoring novel signals found by the *weirddetector* in this work (in decreasing order of  $\zeta_{\text{peak}}$ ).

commensurability between the rotation and orbital period. [Béky et al. \(2014\)](#) proposes an explanation to signals of this nature: if there is a latitude on the surface of a star with a period synchronous to its satellite, magnetic interactions between the objects may result in preferential spot formation at that latitude. The star would then exhibit photometric variations in resonance with its companion.

TIC 197886566 bares some resemblance to this but the phase curve is perhaps more plausibly consistent here with being caused by the companion, although this would require an offset in the phase curve.

Our work provides the first demonstration of an en-masse search for weird signals within the *TESS* photometric data. Although no clear examples of highly irregular signals manifest, the fact we recover 313 EB-like signals and 28 planet-like signals suggests gaps in the completeness func-

tions of standard algorithms and demonstrates the utility of numerous algorithms being applied to photometric data sets such as this

## ACKNOWLEDGMENTS

DMK acknowledges support from the Simons Foundation and the Alfred P. Sloan Foundation. Special thanks to Tom Widdowson, Mark Sloan, Laura Sanborn, Douglas Daughaday, Andrew Jones, Jason Allen, Marc Lijoi, Elena West, Tristan Zajonc, Chuck Wolfred, Lasse Skov & Martin Kroebl.

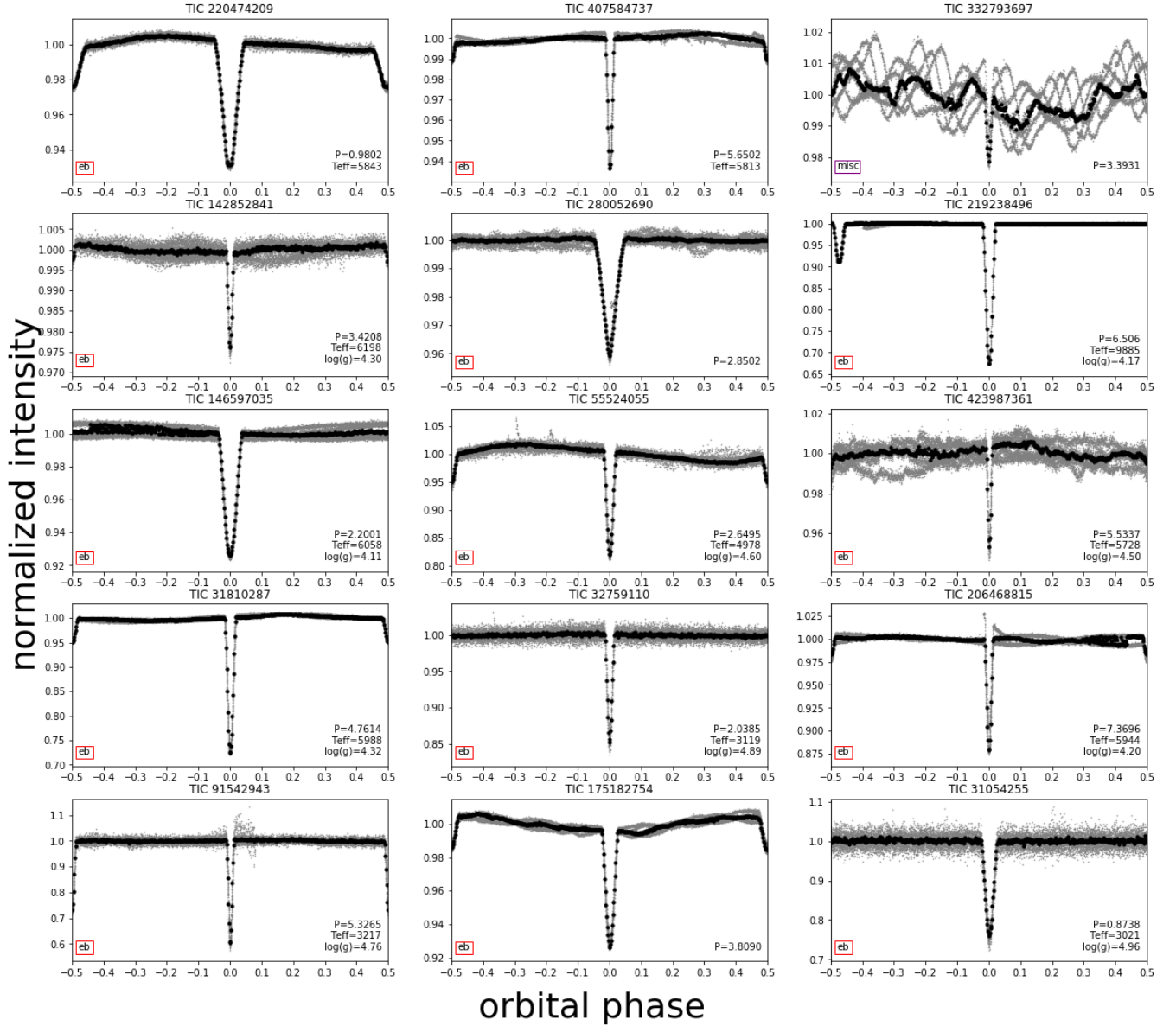


**Figure 4.** The sixteenth to thirtieth highest scoring novel signals found by the `weirddetector` in this work (in decreasing order of  $\zeta_{\text{peak}}$ ).

## DATA AVAILABILITY

The data underlying this article are publicly available at [https://github.com/joheenc/woi\\_data](https://github.com/joheenc/woi_data).

## REFERENCES

- Ballard, S., 2019, *AJ*, 157, 113
- Ballesteros, F. J., Arnalte-Mur, P., Fernandez-Soto, A., Martínez, V. J., 2018, *MNRAS*, 473, 21
- Barclay, T., Pepper, J. & Quintana, E., 2018, *ApJS*, 239, 2
- Béky, B., Holman, M. J., Kipping, D. M., Noyes, R. W., 2014, *ApJ*, 788, 1
- Bodman, E. H. L. & Quillen, A., 2016, *ApJ*, 819, 34
- Bouma, L. G., Winn, J. N., Kosiarek, J., McCullough, P. R., 2017, *arXiv e-prints*:1705.08891
- Boyajian, T. S., LaCourse, D. M., Rappaport, S. A. et al., 2016, *MNRAS*, 457, 3988
- Foreman-Mackey, D., Morton, T. D., Hogg, D. W., Agol, E., Schölkopf, B., 2016, *AJ*, 152, 206
- Foukal, P., 2017, *ApJ*, 842, 3
- Giles, D. & Walkowicz, L., 2019, *MNRAS*, 484, 834
- Jansen, T. & Kipping, D., 2018, *MNRAS*, 478, 3025
- Jayasinghe, T., Kochanek, C. S., Stanek, K. Z., Shappee, B. J., Holoién, T.W., Thompson, T. A., Prieto, J. L., Dong, S., Pawlak, M., Shields, J. V., Pojmanski, G., Otero, S., Britt, C. A., Will, D., 2018, *MNRAS*, 477, 3145
- Jayasinghe, T., Stanek, K. Z., Kochanek, C. S., Shappee, B. J., Holoién, T.W., Thompson, T.A., Prieto, J.L., Dong, S., Pawlak, M., Peicha, O., Shields, J. V., Pojmanski, G., Otero, S., Britt, C. A., Will, D., 2019, *MNRAS*, 486, 1907
- Katz, J. I., 2017, *MNRAS*, 471, 3680
- Kawahara, H. & Masuda, K., 2019, *ApJ*, 157, 218
- Kipping, D. M., Hartman, J., Buchhave, L. A., Schmitt, A. R.,

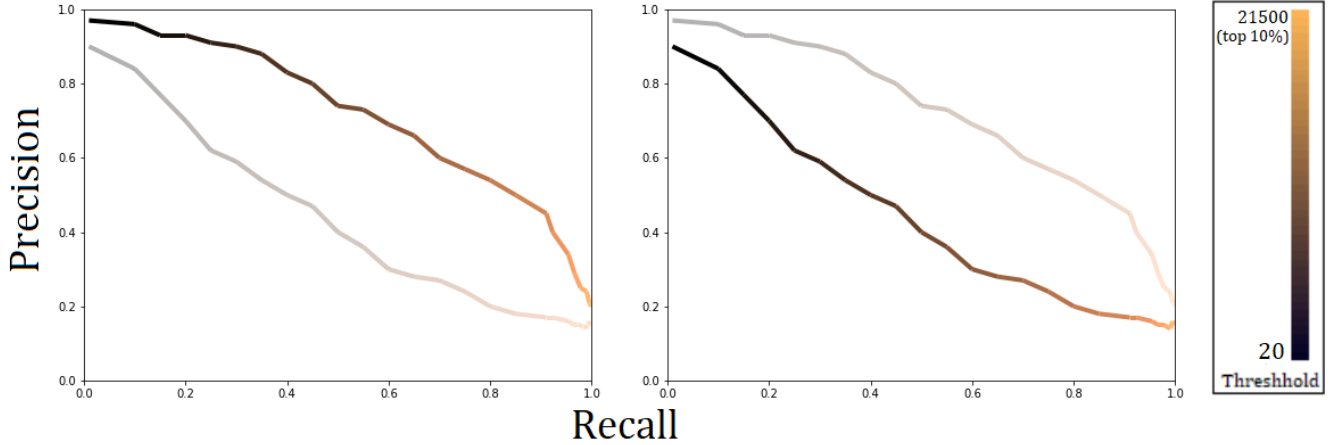


**Figure 5.** Precision-recall curve for our algorithm applied to *TESS* data, with (a) and without (b) cuts. To generate different points, we vary the total number of signals we consider (i.e. the percentile of  $\zeta_{\text{peak}}$  we take for manual triage). To define precision and recall, we take true positives as signals documented in the Villanova eclipsing binaries and *TESS* Objects of Interest, as well as visible signals that passed our data-artifact sanity checks; and false positives as flagged signals not meeting those requirements (most commonly just phase curves with background noise).

- Bakos, G. Á. & Nesvorný, D., 2013, *ApJ*, 770, 101
- Kovács, G., Zucker, S., & Mazeh, T., 2002, *A&A*, 391, 369
- Kovács, G., Zucker, S., & Mazeh, T., 2016, BLS: Box-fitting Least Squares, Astrophysics Source Code Library
- Martinez, M. A. S., Stone, N. C., Metzger, B. D., 2019, *MNRAS*, 489, 5119
- Neslusan, L. & Budaj, J. 2017, *A&A*, 600, 86
- Parks, J. R., Plavchan, P., White, R. J., Gee, A. H., 2014, *ApJS*, 211, 1
- Plavchan, P., Jura, M., Kirkpatrick, J. D., Cutri, R. M., Gallagher, S. C., 2008, *ApJS*, 175, 1
- Prsa, A., 2020, “Eclipsing binary stars: Indispensable astrophysical labs”, *TESS Program G011154*, last accessed 24 June 2020 <https://heasarc.gsfc.nasa.gov/docs/tess/data/approved-programs/G011154.txt>
- Ricker G. R. et al., 2015, *J. Astron. Telesc. Instrum. Syst.*, 1, 014003
- Schmidt, E. G., 2019, *ApJ*, 880, 7
- Schmitt, J. R., Jenkins, J. M. & Fischer, D. A., 2017, *ApJ*, 153, 180
- Shappee, B. J., Prieto, J. L., Grupe, D., Kochanek, C. S., Stanek, K. Z., De Rosa, G., Mathur, S., Zu, Y., Peterson, B. M., Pogge, R. W., Komossa, S., Im, M., Jencson, J., Holoién, T. W., Basu, U., Beacorn, J. F., Szczygiel, D. M., Brimacombe, J., Adams, S., Campillay, A., Choi, C., Contreras, C., Dietrich, M., Dubberley, M., Elphick, M., Foale, S., Giustini, M., Gonzalez, C., Hawkins, E., Howell, D. A., Hsiao, E. Y., Koss, M., Leighly, K. M., Morrell, N., Mudd, D., Mullins, D., Nugent, J. M., Parrent, J., Phillips, M. M., Pojmanski, G., Rosing, W., Ross, R., Sand, D., Terndrup, D. M., Valenti, S., Walker, Z., Yoon, Y., 2014, *ApJ*, 788, 1
- Stassun, K. G., Oelkers, R. J., Pepper, J., et al., 2018, *AJ*, 156, 102
- Sucerquia, M., Alvarado-Montes, J. A., Zuluaga, J. I., Cuello, N., Giuppone, C., 2019, *MNRAS*, 489, 2313
- Sullivan, P. W., Winn, J. N., Berta-Thompson, Z. K. et al., 2015, *ApJ*, 809, 77
- Sullivan, P. W., Winn, J. N., Berta-Thompson, Z. K. et al., 2017, *ApJ*, 837, 99
- Uehara, S., Kawahara, H., Masuda, K., Yamada, S. & Aizawa, M., 2016, *ApJ*, 822, 2
- Wang, J., Fischer, D. A., Barclay, T., et al., 2015, *ApJ*, 815, 127
- Watson, C. L., Henden, A. A., & Price, A., 2006, *The Society for Astronomical Sciences 25th Annual Symposium on Telescope Science*, p.47
- Wheeler, A. & Kipping, D., 2019, *MNRAS*, 485, 5498
- Wright, J. T. & Sigurdsson, S., 2016, *ApJL*, 829, L3
- Wyatt, M. C., van Lieshout, R., Kennedy, G. M. & Boyajian, T. S., 2018, *MNRAS*, 473, 5286



## APPENDIX

Table 1: Parameters for all 377 WOIs (grouped by classification and in descending order by  $\zeta_{\text{peak}}$ .)

TIC ID	$P$ [d]	$\zeta_{\text{peak}}$	$\Delta\chi^2$	$\kappa$	$T_{\text{eff}}$ [K]	$\log g$	dips	$\delta$ [%]	RA	Dec	Flat baseline	Class
468887783	4.5291	1.16e+05	8.20e+03	1.19e+02	6667	3.65	2	14.992	56.67	9.90	y	eb
167692429	10.280	1.07e+05	1.51e+03	1.63e+02	6473	3.48	2	28.962	102.71	-63.43	y	eb
382517745	10.440	1.00e+05	4.85e+02	1.82e+02	5674	4.25	2	12.356	117.45	-64.04	y	eb
180412528	4.5869	9.97e+04	6.50e+03	8.81e+01	—	4.76	2	6.7849	11.35	-77.86	y	eb
133701671	4.6951	9.55e+04	1.55e+04	1.42e+02	7225	4.28	2	10.686	229.68	-48.90	y	eb
149573659	4.3733	9.47e+04	3.70e+03	1.27e+02	5415	4.46	1	11.673	86.61	-61.69	n	eb
260502102	7.3158	9.37e+04	6.17e+03	1.02e+02	5177	4.36	2	17.428	96.51	-59.01	y	eb
363847487	2.4014	8.05e+04	1.12e+04	5.53e+01	6558	4.26	1	6.1775	200.43	-42.62	y	eb
374366829	5.6239	7.86e+04	2.67e+03	1.46e+02	6077	—	2	7.6074	162.71	0.52	y	eb
261335113	8.1311	7.85e+04	1.45e+03	1.53e+02	3347	4.62	2	40.559	92.33	-80.69	y	eb
13957444	3.7405	7.82e+04	2.45e+04	1.00e+02	6313	—	1	8.4917	75.48	-37.03	y	eb
80059889	3.0320	7.74e+04	1.35e+04	7.07e+01	6507	4.09	2	14.450	297.89	-43.37	y	eb
259589049	4.9838	7.67e+04	2.93e+03	1.37e+02	5708	—	1	22.989	72.43	-53.00	y	eb
260504147	8.418	7.43e+04	5.35e+04	1.12e+02	—	—	1	17.577	96.43	-55.16	y	eb
308851582	4.9114	7.05e+04	1.09e+03	1.18e+02	5916	4.47	2	20.297	122.58	-63.74	y	eb
220474209	0.9802	6.84e+04	1.22e+05	3.09e+01	5843	—	2	6.9241	75.38	-59.51	y	eb
407584737	5.6502	6.77e+04	1.80e+04	1.60e+02	5813	—	2	6.3343	352.77	-74.13	y	eb
332793697	3.3931	6.64e+04	4.16e+03	5.97e+01	—	—	1	2.0910	215.98	-50.49	n	misc
142852841	3.4208	6.54e+04	4.29e+03	8.79e+01	6198	4.30	2	2.4215	50.50	-31.10	y	eb
280052690	2.8502	6.52e+04	4.10e+03	9.08e+01	—	—	1	4.0962	45.44	-76.20	y	eb
219238496	6.506	6.49e+04	8.86e+03	2.06e+02	9885	4.17	2	32.689	64.49	-48.39	y	eb
146597035	2.2001	6.37e+04	1.34e+04	8.37e+01	6058	4.11	1	7.3864	77.77	-21.49	y	eb
55524055	2.6495	6.34e+04	1.16e+04	7.65e+01	4978	4.60	2	18.112	72.05	-63.69	y	eb
423987361	5.5337	6.20e+04	3.27e+03	1.36e+02	5728	4.50	1	4.6543	235.84	-63.66	n	eb
31810287	4.7614	5.85e+04	3.13e+04	1.21e+02	5988	4.32	2	27.721	136.65	-47.06	y	eb
32759110	2.0385	5.79e+04	1.55e+04	8.20e+01	3119	4.89	1	14.696	86.24	-24.93	y	eb
206468815	7.3696	5.77e+04	2.61e+03	1.43e+02	5944	4.20	2	12.202	57.01	-53.60	y	eb
91542943	5.3265	5.67e+04	5.11e+03	1.05e+02	3217	4.76	1	40.042	43.82	-33.74	y	eb
175182754	3.8090	5.65e+04	6.71e+03	1.08e+02	—	—	2	7.3807	115.96	-37.72	y	eb
31054255	0.8738	5.52e+04	1.45e+04	2.74e+01	3021	4.96	1	24.747	80.57	-25.11	y	eb
178938417	5.9747	5.48e+04	6.48e+03	1.98e+02	5405	4.51	2	0.8074	68.27	-24.01	n	eb
142409400	1.3869	5.42e+04	1.74e+04	2.59e+01	3385	4.58	2	19.947	103.09	-12.96	y	eb
178284729	2.2360	5.41e+04	2.78e+03	7.51e+01	3968	4.63	1	11.031	60.38	-20.45	y	eb
32150630	1.4921	5.38e+04	1.84e+04	4.36e+01	4323	—	2	14.503	59.24	-68.62	n	eb
143924219	2.8199	5.35e+04	4.54e+03	7.65e+01	6412	3.99	1	2.5442	332.70	-48.89	n	eb
339607421	2.4381	5.25e+04	1.33e+04	8.03e+01	6327	4.33	1	5.4663	46.20	-52.55	y	eb
238162238	1.2186	5.10e+04	3.65e+04	4.54e+01	6172	4.14	2	4.2458	106.39	-48.84	n	eb
421285598	2.3578	5.07e+04	4.77e+03	4.61e+01	5745	4.15	2	13.222	261.92	-54.11	n	eb
49534600	7.9529	5.06e+04	2.42e+03	1.52e+02	—	—	2	15.235	273.69	-52.81	y	eb
301956407	1.8314	4.99e+04	2.86e+04	5.52e+01	6079	4.09	2	2.6056	260.05	-70.04	y	eb
423530755	2.3421	4.97e+04	3.41e+04	8.64e+01	5547	4.27	1	7.2387	185.30	-20.70	n	eb
365694569	9.0344	4.88e+04	3.69e+04	1.13e+02	6358	3.99	2	34.617	81.63	9.69	y	eb
147975720	2.8502	4.88e+04	1.37e+04	9.88e+01	3464	4.73	1	27.351	99.59	-37.24	y	eb
33912852	1.7049	4.78e+04	6.74e+04	3.69e+01	6541	4.06	2	1.9524	356.14	-26.47	y	eb
35349987	10.738	4.75e+04	1.33e+03	1.92e+02	3721	4.57	1	19.456	224.78	-55.66	y	eb
101845679	1.2811	4.72e+04	3.69e+04	2.44e+01	6252	4.06	2	1.5564	304.00	-50.13	y	eb
178171080	3.2501	4.71e+04	2.40e+03	1.00e+02	—	—	1	2.4862	43.26	-31.40	n	eb
49558810	3.3543	4.58e+04	4.31e+03	8.50e+01	5209	4.34	1	7.8446	36.53	-36.37	y	eb
290476605	5.7452	4.52e+04	1.24e+04	1.60e+02	6687	3.96	2	2.7871	139.16	0.72	y	eb
140659978	9.4407	4.46e+04	2.25e+03	1.41e+02	5221	4.20	2	29.384	72.45	-72.46	y	eb
278784173	0.7473	4.45e+04	2.43e+04	3.31e+01	—	—	1	6.3155	335.73	-37.52	y	eb
250387838	6.8863	4.40e+04	1.08e+04	1.09e+02	5871	3.80	2	3.7178	30.26	-2.49	y	eb
371839073	3.7963	4.38e+04	2.74e+03	9.26e+01	6034	4.22	1	10.071	306.00	-71.08	y	eb
269852699	5.1365	4.38e+04	2.12e+03	7.51e+01	6137	4.13	2	11.706	69.88	-79.72	y	eb

Table 1: *Parameters for all 377 WOIs (grouped by classification and in descending order by  $\zeta_{\text{peak}}$ .)*

TIC ID	$P$ [d]	$\zeta_{\text{peak}}$	$\Delta\chi^2$	$\kappa$	$T_{\text{eff}}$ [K]	$\log g$	dips	$\delta$ [%]	RA	Dec	Flat baseline	Class
220397947	1.7757	4.30e+04	3.94e+03	5.98e+01	6257	4.01	1	7.2456	69.01	-58.07	y	eb
340100436	1.4689	4.30e+04	1.17e+04	5.98e+01	5297	4.43	1	3.9916	237.69	-63.97	y	eb
379783522	2.4499	4.23e+04	1.91e+04	4.14e+01	—	—	2	1.6508	181.59	-65.70	n	eb
255700967	3.4253	4.23e+04	2.56e+03	1.00e+02	6896	3.94	1	4.4857	98.90	-52.33	y	eb
201747686	1.3457	4.20e+04	1.60e+04	3.02e+01	6233	—	2	2.2124	303.47	-57.99	n	eb
273792220	1.9879	4.19e+04	2.99e+05	3.61e+01	5892	4.13	2	6.4483	30.55	-62.59	n	eb
158150633	2.0783	4.13e+04	3.24e+03	5.82e+01	4525	—	2	11.701	162.13	-38.90	n	eb
250196734	7.7037	4.11e+04	1.94e+05	1.41e+02	3962	4.41	2	50.505	65.21	-2.62	y	eb
102691227	1.2097	4.10e+04	6.55e+04	4.60e+01	6457	4.05	1	7.4433	155.57	-43.21	y	eb
146522930	1.0875	4.09e+04	8.56e+03	2.10e+01	5812	—	2	4.0696	76.69	-19.96	y	eb
278706358	3.4512	4.08e+04	3.42e+04	1.15e+02	5619	4.11	2	36.414	334.81	-40.53	y	eb
55369219	1.9793	4.06e+04	5.22e+03	4.54e+01	6821	3.82	1	7.4981	77.50	-61.59	y	eb
348759510	3.7162	4.04e+04	2.43e+04	1.41e+02	6672	4.28	1	2.9118	134.20	-17.43	y	eb
253715855	1.1317	4.02e+04	1.88e+04	3.82e+01	6138	4.20	2	4.3179	282.06	-37.18	n	eb
158582801	1.0801	4.02e+04	4.98e+05	3.78e+01	—	—	1	43.263	21.86	-49.47	y	eb
219362976	7.9768	4.01e+04	4.65e+03	2.11e+02	4387	4.29	1	20.637	75.11	-49.42	y	eb
237944385	4.4247	4.00e+04	1.97e+03	1.52e+02	6304	4.03	1	1.7937	101.22	-48.70	y	pl
201293780	0.9377	4.00e+04	3.04e+04	2.45e+01	5962	4.29	2	1.7623	3.23	-57.35	y	eb
436158814	7.2141	3.99e+04	1.85e+03	1.27e+02	3510	4.64	2	19.849	83.94	9.76	y	eb
176591772	7.7591	3.94e+04	1.68e+03	1.03e+02	5626	4.19	2	6.9878	87.57	-5.77	y	eb
148612685	5.0098	3.88e+04	6.32e+04	9.22e+01	—	—	2	12.547	165.34	-11.89	y	eb
293081694	1.2540	3.83e+04	1.95e+04	3.80e+01	6335	4.19	2	3.1344	175.04	-27.26	n	eb
92594505	11.435	3.79e+04	1.38e+03	1.72e+02	6302	3.75	1	7.8543	315.46	-33.48	y	eb
231293332	1.7879	3.78e+04	5.31e+04	6.50e+01	6140	4.22	1	15.375	44.71	-49.17	y	eb
88380001	4.4343	3.74e+04	2.42e+03	1.15e+02	6458	4.10	1	1.7522	44.79	-25.23	y	pl
231809798	0.9057	3.63e+04	9.96e+04	1.99e+01	3520	4.74	2	18.734	85.53	-52.11	y	eb
281494100	2.3076	3.63e+04	2.38e+05	6.51e+01	6427	4.17	2	43.686	112.19	-56.40	y	eb
253657883	0.7908	3.62e+04	9.50e+03	2.08e+01	4316	4.51	2	8.2538	281.47	-39.41	n	eb
140659980	9.4392	3.57e+04	1.88e+03	1.63e+02	5642	3.84	2	5.3466	72.47	-72.46	n	eb
387544749	2.8185	3.55e+04	3.55e+04	6.12e+01	3711	4.59	2	9.5871	44.25	10.31	n	eb
143022688	1.5663	3.55e+04	2.12e+05	5.30e+01	4086	—	2	12.777	54.26	-30.07	y	eb
117739806	5.6174	3.55e+04	8.52e+02	1.14e+02	5981	4.39	2	20.181	96.20	-31.86	y	eb
278861826	0.5337	3.47e+04	2.79e+04	1.58e+01	6369	4.03	1	3.7808	100.65	-56.54	y	eb
52641430	1.6715	3.47e+04	9.45e+03	2.90e+01	—	—	2	1.6214	101.11	-33.98	n	eb
39818458	3.8154	3.44e+04	1.85e+04	1.25e+02	12561	—	1	5.3337	90.19	-3.89	y	eb
211116547	1.2768	3.44e+04	1.43e+04	2.92e+01	—	4.74	2	36.378	280.43	-31.67	y	eb
333642126	4.827	3.41e+04	1.45e+03	9.64e+01	5051	4.30	1	11.344	56.36	-4.12	y	eb
48658291	1.5878	3.40e+04	2.00e+04	6.16e+01	6322	3.74	1	8.8601	96.92	-25.83	y	eb
198076334	0.3913	3.39e+04	2.74e+05	1.53e+01	5854	3.61	1	2.4643	63.65	-59.08	y	eb
3921749	5.6108	3.39e+04	5.66e+04	1.34e+02	4007	4.38	1	33.918	11.83	-6.44	y	eb
253749178	1.8377	3.38e+04	4.19e+03	5.09e+01	5958	—	2	10.192	282.34	-36.76	n	eb
310556491	1.5554	3.28e+04	6.39e+04	4.03e+01	6902	4.15	2	5.2244	185.28	-65.83	n	eb
77437462	0.6079	3.27e+04	5.41e+03	3.11e+01	3588	4.77	1	1.8442	73.13	-36.53	n	pl
294059372	0.6666	3.26e+04	3.27e+04	1.95e+01	6393	—	2	7.1110	263.93	-71.40	n	eb
300972613	0.3880	3.25e+04	1.34e+05	1.30e+01	—	—	2	6.5351	10.77	-47.30	y	eb
357911163	4.7821	3.22e+04	2.19e+04	8.52e+01	6682	4.42	2	15.130	192.89	-79.02	y	eb
25188036	3.3930	3.18e+04	1.21e+03	4.41e+01	2868	5.05	2	1009.9	98.02	-7.31	y	eb
268587594	9.1404	3.18e+04	2.40e+03	2.00e+02	5887	4.19	3	3.8126	15.73	-23.88	n	misc
278826996	9.5834	3.16e+04	1.39e+03	1.77e+02	5800	4.03	2	35.039	100.33	-54.02	y	eb
52641431	0.8358	3.16e+04	7.13e+03	2.25e+01	—	—	2	1.5964	101.11	-33.98	n	eb
434664688	8.4292	3.09e+04	1.90e+03	1.54e+02	—	—	2	18.548	191.23	-65.31	y	eb
142148228	0.7805	3.06e+04	9.43e+03	2.27e+01	6775	4.08	1	0.6429	100.36	-74.67	n	pl
150357064	1.4894	3.03e+04	3.55e+03	4.98e+01	5722	4.13	1	5.8414	96.10	-64.49	n	eb
243475355	1.0957	3.03e+04	1.26e+04	3.07e+01	13560	—	2	1.2504	205.91	-42.06	y	eb
146439804	11.014	3.03e+04	6.27e+02	1.74e+02	3801	4.32	1	10.465	75.73	-22.22	y	eb
262696097	0.9111	3.03e+04	7.64e+03	2.69e+01	6782	3.79	1	3.1139	107.78	7.45	n	eb

Table 1: *Parameters for all 377 WOIs (grouped by classification and in descending order by  $\zeta_{\text{peak}}$ .)*

TIC ID	$P$ [d]	$\zeta_{\text{peak}}$	$\Delta\chi^2$	$\kappa$	$T_{\text{eff}}$ [K]	$\log g$	dips	$\delta$ [%]	RA	Dec	Flat baseline	Class
424992973	6.9254	3.02e+04	6.41e+03	1.83e+02	5171	—	2	35.136	81.80	-18.57	y	eb
38937499	2.0276	3.00e+04	2.65e+03	5.70e+01	5199	4.32	2	0.3917	10.30	-68.45	y	eb
79548760	7.9728	2.98e+04	9.98e+02	1.43e+02	6452	3.66	1	4.0596	51.07	-45.09	y	eb
143171265	1.1410	2.97e+04	1.22e+04	3.72e+01	7333	4.31	2	1.7917	89.99	-34.45	n	eb
294092960	0.9022	2.97e+04	1.54e+04	2.23e+01	5766	4.57	2	5.0331	107.35	-57.50	n	eb
146688260	0.5030	2.94e+04	3.01e+04	1.53e+01	5551	4.28	2	1.3734	43.22	-43.52	n	eb
58466459	3.8717	2.93e+04	6.87e+02	6.60e+01	6398	4.09	2	7.2758	201.66	-27.14	y	eb
148544875	1.7441	2.92e+04	8.11e+03	6.30e+01	3159	4.88	1	24.273	164.12	-9.83	y	eb
332488398	1.0416	2.92e+04	8.54e+04	2.70e+01	5458	4.29	1	4.7379	350.56	-29.70	y	eb
281728376	11.177	2.91e+04	8.26e+02	1.73e+02	6656	4.00	1	2.6819	11.65	-54.10	y	eb
317411334	1.4485	2.89e+04	1.48e+04	4.88e+01	6036	4.15	1	8.9622	87.71	-12.15	y	eb
53997651	1.4587	2.86e+04	4.79e+04	6.27e+01	3418	4.71	1	73.489	159.57	-33.26	y	eb
441422220	3.6995	2.81e+04	6.93e+03	1.13e+02	6348	4.26	2	28.628	311.36	-34.64	y	eb
284196801	11.158	2.80e+04	1.03e+03	1.72e+02	6098	3.77	2	3.6876	105.54	-71.12	y	eb
90716944	8.0234	2.79e+04	6.12e+03	2.12e+02	4900	4.55	2	15.891	277.08	-45.49	y	eb
386262459	2.6672	2.79e+04	2.00e+03	8.05e+01	9557	4.15	2	1.9070	127.40	-16.00	n	eb
91246422	9.4234	2.76e+04	2.73e+03	1.61e+02	12417	—	1	4.2674	277.93	-45.91	y	eb
278826516	7.0430	2.75e+04	5.33e+02	1.24e+02	6248	4.10	1	10.377	100.47	-54.81	y	eb
91636891	13.450	2.74e+04	9.44e+02	1.61e+02	6461	3.91	1	20.549	39.40	-36.97	y	eb
153742549	6.0700	2.74e+04	2.10e+03	8.23e+01	5726	3.63	2	11.324	66.52	-44.59	y	eb
178723395	1.7616	2.70e+04	2.30e+03	5.09e+01	6756	4.26	1	4.0281	166.14	-43.24	y	eb
279949020	6.5493	2.65e+04	1.04e+03	1.37e+02	5860	3.77	2	14.611	40.39	-59.98	y	eb
207080350	9.1069	2.65e+04	3.52e+05	1.93e+02	6978	3.98	2	33.987	320.91	-39.77	y	eb
27654882	1.1156	2.65e+04	2.99e+03	3.74e+01	6447	3.88	1	3.4932	123.70	12.06	y	eb
270204401	2.2383	2.64e+04	3.58e+03	4.77e+01	9428	4.19	2	17.609	332.71	-71.97	y	eb
350297040	10.874	2.63e+04	4.47e+02	1.27e+02	6294	4.45	2	19.383	83.71	-55.93	y	eb
12158853	0.6311	2.61e+04	2.55e+05	2.17e+01	3465	4.69	2	18.312	91.55	-3.61	y	eb
218152299	1.2597	2.59e+04	1.63e+04	3.65e+01	6225	3.83	1	7.6603	261.91	-45.55	y	eb
2372579	9.9215	2.58e+04	2.30e+03	2.16e+02	5417	4.22	1	16.004	288.91	-28.68	y	eb
32449963	6.5199	2.58e+04	5.22e+04	1.91e+02	5771	4.27	2	31.714	189.93	-11.64	y	eb
70717462	2.9482	2.52e+04	2.18e+03	8.70e+01	—	—	1	2.2676	151.63	-35.18	n	eb
426541180	4.6975	2.50e+04	1.15e+03	9.95e+01	5715	4.32	1	4.7776	244.93	-72.21	n	eb
358108063	2.9858	2.49e+04	1.06e+03	7.24e+01	5723	—	2	8.8750	51.24	-75.93	y	eb
394585218	3.9645	2.48e+04	1.46e+03	9.38e+01	6032	3.99	2	8.3107	341.02	-65.76	y	eb
178996712	2.9828	2.46e+04	1.46e+04	4.16e+01	7188	4.10	2	3.6709	70.06	-27.73	n	eb
220359766	1.7599	2.45e+04	2.14e+03	4.65e+01	—	—	1	2.2444	155.05	-52.19	y	eb
341309569	7.3475	2.45e+04	6.00e+02	1.24e+02	4966	—	1	4.7958	315.92	-64.13	n	eb
139188326	0.5883	2.42e+04	8.99e+04	1.08e+01	6506	3.67	2	0.7701	345.01	-46.49	n	eb
270166263	7.6589	2.41e+04	2.03e+03	1.63e+02	4933	4.13	2	11.119	330.03	-27.70	y	eb
317191077	2.1910	2.41e+04	4.85e+03	4.17e+01	6364	—	2	4.7310	87.14	-13.05	n	eb
409900613	1.1032	2.40e+04	9.07e+03	4.67e+01	3194	4.83	1	9.5539	144.89	-17.59	y	eb
118200081	0.9529	2.39e+04	1.01e+04	1.79e+01	5366	—	2	3.4996	272.18	-56.78	n	eb
115275539	1.7630	2.37e+04	3.17e+03	5.11e+01	4913	—	1	2.3541	25.95	-38.72	y	eb
46313508	1.0326	2.33e+04	6.23e+03	2.50e+01	6445	3.60	2	2.3889	83.10	-14.97	n	eb
124350360	8.5580	2.33e+04	2.38e+04	2.33e+02	3471	4.62	1	14.902	227.66	-52.80	y	eb
169316288	0.5589	2.33e+04	4.26e+04	1.42e+01	6290	—	2	5.4193	292.50	-27.95	n	eb
222945452	0.7483	2.31e+04	1.41e+04	2.12e+01	—	—	2	0.9521	245.89	-44.11	n	eb
228760807	0.7779	2.30e+04	9.22e+04	2.03e+01	5320	—	2	3.9835	194.10	-27.39	y	eb
396655059	7.9781	2.30e+04	1.17e+03	1.00e+02	7909	4.16	2	12.262	214.77	-77.09	y	eb
440788366	0.7742	2.28e+04	6.48e+03	2.05e+01	9079	—	1	2.6778	109.09	12.45	n	eb
18914916	11.287	2.27e+04	5.66e+02	1.51e+02	5486	4.57	2	15.729	118.92	13.80	y	eb
180943676	8.418	2.26e+04	8.62e+02	1.52e+02	6027	4.39	1	8.2751	88.72	-46.42	n	eb
294197236	0.9672	2.24e+04	4.36e+03	3.07e+01	6372	3.60	1	5.6588	264.81	-68.78	n	eb
312111256	1.1517	2.19e+04	1.01e+04	2.71e+01	7593	4.38	2	3.6697	140.66	6.23	n	eb
423524230	2.5815	2.18e+04	1.32e+03	6.25e+01	6564	4.33	2	2.7988	169.18	-19.89	n	eb
30382918	0.5719	2.17e+04	2.86e+05	1.04e+01	5854	4.22	2	3.3986	198.43	-41.27	y	eb

Table 1: *Parameters for all 377 WOIs (grouped by classification and in descending order by  $\zeta_{\text{peak}}$ .)*

TIC ID	$P$ [d]	$\zeta_{\text{peak}}$	$\Delta\chi^2$	$\kappa$	$T_{\text{eff}}$ [K]	$\log g$	dips	$\delta$ [%]	RA	Dec	Flat baseline	Class
48063034	0.5863	2.16e+04	5.19e+04	1.52e+01	5304	4.20	2	6.5276	147.48	-34.11	n	eb
67267845	1.0126	2.16e+04	4.29e+03	3.57e+01	6817	3.64	1	11.205	240.95	-29.97	n	eb
35101462	4.1726	2.16e+04	1.76e+03	7.34e+01	6114	4.21	2	5.3038	35.41	-14.78	y	eb
363933313	4.6865	2.13e+04	9.98e+02	9.37e+01	5428	—	1	11.931	251.32	-71.05	y	eb
270411008	8.6657	2.11e+04	2.14e+04	2.31e+02	5492	4.24	1	41.883	349.40	-29.17	y	eb
301247295	8.5054	2.10e+04	1.47e+03	9.64e+01	5933	—	2	15.232	255.08	-69.56	y	eb
244163413	1.7879	2.09e+04	8.52e+04	6.67e+01	6098	4.29	2	14.971	5.16	-5.14	y	eb
468958384	0.7675	2.07e+04	4.07e+03	2.16e+01	3478	4.81	1	35.711	107.70	7.90	y	eb
146761368	0.9176	2.05e+04	3.53e+03	2.83e+01	6597	3.58	1	6.5819	46.17	-44.66	n	eb
191926695	1.9352	2.02e+04	9.92e+03	3.56e+01	—	—	2	2.2496	136.52	-38.88	y	eb
303427297	4.2976	2.02e+04	1.29e+03	5.27e+01	5273	—	2	1.7764	164.18	-57.75	n	eb
260659986	3.5699	2.01e+04	9.93e+02	9.34e+01	6107	3.90	1	16.691	98.48	-59.96	y	eb
117879940	1.1311	2.00e+04	3.29e+03	2.72e+01	5559	3.92	2	3.8599	70.72	-11.87	n	eb
380645083	4.3894	1.99e+04	1.95e+03	8.61e+01	5927	3.58	2	0.9681	285.20	-34.88	n	eb
259864042	0.4607	1.99e+04	2.81e+03	3.90e+01	31000	5.59	1	14.676	40.32	-68.92	n	eb
234494090	0.9726	1.96e+04	3.10e+03	2.98e+01	—	—	1	19.558	9.81	-63.20	y	eb
319467578	2.3652	1.93e+04	1.48e+03	4.72e+01	6157	4.22	2	2.4735	100.22	-52.69	y	eb
369966331	0.9128	1.92e+04	8.60e+03	1.77e+01	4686	—	2	0.9706	19.73	-65.18	y	eb
291320884	0.3717	1.88e+04	3.30e+05	8.40e+00	3507	4.73	2	33.227	260.95	-57.41	n	eb
410654298	8.2252	1.79e+04	1.91e+04	2.18e+02	5234	—	1	18.858	177.00	-66.11	y	eb
66509654	2.6446	1.76e+04	3.45e+03	9.16e+01	3253	4.80	1	35.119	109.42	-23.99	y	eb
22937402	1.3839	1.76e+04	1.59e+04	2.29e+01	—	—	2	0.6199	109.13	-38.31	n	eb
94257578	1.1921	1.74e+04	2.43e+03	5.15e+01	5722	—	2	3.2446	241.41	-30.64	n	eb
263925187	0.3330	1.73e+04	2.71e+04	1.21e+01	3944	4.59	1	21.136	269.99	-30.07	n	eb
9053429	12.962	1.72e+04	6.14e+02	1.30e+02	31000	5.59	1	33.615	356.09	-10.19	y	eb
197886566	0.8721	1.71e+04	1.32e+04	1.45e+01	6019	4.04	1	1.1038	57.31	-58.44	n	pl
11756637	4.3061	1.70e+04	2.38e+04	9.04e+01	3436	4.60	2	53.312	90.61	-1.31	y	eb
78450017	0.9438	1.70e+04	2.19e+03	2.75e+01	3524	4.60	1	11.030	102.58	-21.46	y	eb
259543079	9.0208	1.69e+04	5.39e+02	1.24e+02	5241	4.31	1	17.720	71.63	-53.12	y	eb
365570620	0.8584	1.69e+04	3.59e+03	2.69e+01	6505	3.73	1	4.8005	81.29	7.95	n	eb
142177867	1.4353	1.65e+04	7.92e+04	3.44e+01	5456	4.33	2	3.8672	37.41	-47.22	y	eb
61724376	0.9538	1.64e+04	3.60e+03	2.46e+01	5780	3.82	1	5.1693	288.95	-44.50	n	eb
220015845	54.515	1.64e+04	2.43e+03	2.10e+02	5950	4.12	1	33.659	32.36	-49.55	n	eb
173038281	4.309	1.64e+04	1.00e+03	8.94e+01	6412	4.22	1	1.8536	102.27	-27.34	y	pl
60479151	0.4189	1.63e+04	1.03e+04	1.46e+01	6210	3.99	1	1.6225	96.31	-21.78	y	pl
164681172	4.9064	1.61e+04	4.12e+04	1.09e+02	5694	4.23	2	31.586	24.56	-21.07	y	eb
91961	5.2823	1.56e+04	9.56e+02	8.55e+01	—	4.83	2	18.651	221.69	-23.91	y	eb
31690845	1.1991	1.54e+04	6.68e+03	1.77e+01	6652	3.43	2	2.2371	289.12	-31.40	n	eb
48063032	0.5863	1.54e+04	2.84e+04	1.51e+01	5824	4.39	2	5.3075	147.48	-34.11	n	eb
162585282	0.5122	1.53e+04	1.02e+05	8.79e+00	3311	4.75	2	31.019	170.31	-47.58	n	eb
4723156	9.4896	1.51e+04	4.85e+04	1.72e+02	3057	4.96	2	41.058	39.44	-7.09	y	eb
323295967	0.4245	1.50e+04	1.59e+04	1.15e+01	5581	—	2	1.8769	52.64	-39.24	n	eb
219328784	1.9687	1.47e+04	1.55e+03	4.42e+01	4539	4.30	1	1.0865	333.50	-54.11	n	eb
18915591	3.4933	1.45e+04	8.48e+02	8.28e+01	7432	3.41	1	21.963	118.91	12.66	y	eb
12631605	0.7086	1.44e+04	1.28e+05	1.66e+01	5514	4.44	2	20.219	53.11	-6.97	y	eb
147314529	0.4628	1.40e+04	1.08e+04	1.67e+01	11310	3.70	1	1.3431	104.69	-17.63	n	pl
340633943	0.3757	1.40e+04	4.79e+04	9.30e+00	6031	4.41	1	6.0757	116.49	-56.54	n	eb
412345587	0.5268	1.38e+04	3.06e+04	1.72e+01	3516	4.82	1	121.13	110.53	-18.64	n	eb
114819301	4.8876	1.37e+04	8.06e+02	7.87e+01	3786	4.32	1	6.2994	2.30	-18.91	y	eb
401926767	6.8009	1.36e+04	1.26e+05	1.20e+02	4342	4.25	2	48.278	57.35	-1.24	y	eb
52924466	10.612	1.34e+04	3.99e+02	1.31e+02	5305	4.43	1	3.5125	102.38	-33.70	y	eb
350298314	13.525	1.33e+04	3.58e+02	1.22e+02	5468	4.59	1	23.465	83.74	-59.33	y	eb
183537458	0.2278	1.32e+04	2.00e+05	7.49e+00	6283	4.42	1	1.8545	357.79	-39.86	y	usp
159897979	16.785	1.29e+04	1.29e+03	1.12e+02	6687	3.74	2	20.779	48.84	-38.99	y	eb
343757299	5.8194	1.28e+04	9.17e+02	7.35e+01	9787	4.00	1	5.1452	273.21	-74.28	y	eb
219201178	2.4170	1.28e+04	7.41e+02	4.50e+01	6760	4.03	2	3.6424	92.72	-52.89	n	eb



Table 1: Parameters for all 377 WOIs (grouped by classification and in descending order by  $\zeta_{\text{peak}}$ .)

TIC ID	$P$ [d]	$\zeta_{\text{peak}}$	$\Delta\chi^2$	$\kappa$	$T_{\text{eff}}$ [K]	$\log g$	dips	$\delta$ [%]	RA	Dec	Flat baseline	Class
148611095	4.8374	1.27e+04	1.01e+04	5.47e+01	3452	4.78	2	13.377	165.21	-7.26	y	eb
143234741	1.9178	1.27e+04	7.46e+02	3.75e+01	5855	4.17	1	3.5656	90.62	-32.38	n	eb
167812449	4.2356	1.25e+04	4.60e+02	7.52e+01	5799	4.28	2	1.7238	104.78	-61.84	n	eb
269996393	10.381	1.25e+04	4.94e+02	1.28e+02	5711	4.51	1	0.5600	311.46	-27.60	n	misc
358022169	0.3032	1.24e+04	3.48e+04	8.15e+00	5740	4.53	2	0.5261	193.65	-80.07	y	eb
159803421	0.2761	1.24e+04	1.32e+04	1.23e+01	5708	4.37	1	0.2218	261.64	-32.96	y	usp
120566395	1.7957	1.23e+04	1.72e+03	2.67e+01	6001	4.04	1	1.3061	3.84	-39.52	n	pl
124712813	0.8256	1.23e+04	2.30e+03	2.07e+01	3592	4.68	2	7.0125	104.76	-11.72	n	eb
326356701	1.1122	1.20e+04	4.50e+03	2.18e+01	4674	—	2	1.5596	325.59	-21.76	n	eb
355357949	1.4604	1.17e+04	1.20e+03	3.51e+01	6714	4.17	1	3.5642	109.33	-49.41	n	eb
47175622	1.5235	1.16e+04	2.62e+03	2.84e+01	6698	—	2	1.5101	145.35	-7.65	y	eb
293480903	7.5701	1.11e+04	5.00e+02	7.90e+01	6180	—	2	3.4731	49.97	-82.14	n	eb
63037741	12.295	1.09e+04	3.03e+02	1.52e+02	3341	4.84	1	6.5	336.86	-35.01	y	misc
266769521	0.5362	1.07e+04	1.72e+06	7.77e+00	6659	4.06	2	36.167	29.75	-22.91	n	eb
265551788	10.943	1.04e+04	3.55e+02	1.19e+02	5258	—	1	1.4161	94.75	5.93	y	pl
21184505	5.1777	1.02e+04	6.55e+02	1.01e+02	6146	4.23	3	0.7600	128.85	12.01	n	eb
443494351	0.2578	1.02e+04	3.05e+04	7.87e+00	7620	3.33	1	1.8084	146.78	-54.20	n	usp
425864141	0.1091	1.01e+04	1.60e+05	6.38e+00	3039	4.92	1	15.052	352.08	-45.91	n	usp
76698707	0.2639	1.01e+04	1.44e+04	9.62e+00	5845	3.61	1	1.1410	229.05	-32.49	y	usp
300560295	10.292	1.00e+04	2.55e+02	1.00e+02	5885	4.25	1	2.3754	112.91	-68.13	n	eb
274229418	9.6186	1.00e+04	1.16e+04	2.37e+02	3422	4.76	1	28.221	115.47	5.04	y	eb
278683641	4.2420	9.98e+03	1.09e+03	5.11e+01	6095	4.03	2	14.176	99.24	-58.46	y	eb
349970685	1.2570	9.95e+03	1.15e+03	2.03e+01	—	—	2	9.6550	114.48	-60.29	y	eb
75352949	0.4720	9.84e+03	5.46e+04	8.10e+00	4816	—	2	4.3822	6.41	-17.81	n	eb
150357290	0.4926	9.81e+03	4.92e+03	1.36e+01	5650	4.39	1	0.6642	96.16	-64.05	n	misc
224283342	0.8873	9.74e+03	6.83e+03	1.16e+01	3165	4.88	3	5.1680	356.35	-40.33	n	misc
56128191	3.1118	9.72e+03	6.14e+02	5.59e+01	6798	4.20	2	2.9522	70.75	-6.43	y	eb
133105082	0.4464	9.41e+03	3.23e+04	5.79e+00	3282	4.74	2	307.51	120.46	-40.50	n	eb
309025566	8.8084	9.41e+03	5.13e+04	2.38e+02	6459	—	1	13.707	151.07	-28.37	y	eb
384742846	6.3568	9.34e+03	6.43e+02	6.10e+01	6542	4.20	2	19.510	258.72	-82.85	y	eb
173077938	1.2970	9.33e+03	3.07e+03	1.66e+01	7382	3.87	2	0.3219	111.05	-40.86	n	eb
254039358	0.7477	9.16e+03	2.33e+03	1.60e+01	6124	4.10	1	0.4260	285.25	-40.38	y	pl
121048789	0.6441	9.16e+03	4.15e+03	1.80e+01	5709	4.21	1	0.3975	56.19	-21.29	y	pl
308184924	4.1283	8.89e+03	7.20e+02	4.39e+01	6082	3.99	2	26.963	130.43	-69.78	y	eb
153709888	2.1663	8.85e+03	9.29e+02	3.93e+01	6720	4.22	1	6.3590	65.56	-42.07	y	eb
304071827	1.5913	8.78e+03	2.92e+03	2.34e+01	6645	3.97	1	0.4086	258.45	-65.68	n	pl
22146154	6.0609	8.58e+03	2.79e+02	8.65e+01	6874	3.97	1	2.9735	148.76	-25.13	y	eb
189639080	1.5666	8.36e+03	4.35e+02	3.27e+01	8840	—	1	18.359	144.21	-28.48	y	eb
32050581	1.5564	8.30e+03	5.09e+02	3.36e+01	5503	4.22	1	2.4356	57.07	-69.15	y	eb
98658304	5.9320	8.29e+03	5.72e+02	7.09e+01	4996	—	2	15.442	8.93	-22.74	n	eb
220569051	2.7779	8.25e+03	6.91e+02	4.67e+01	6025	3.73	2	6.6498	46.36	-60.36	y	eb
55659311	5.595	7.96e+03	3.12e+02	6.63e+01	5103	4.45	2	20.880	74.11	-64.48	y	eb
408512382	4.0311	7.96e+03	7.19e+02	6.06e+01	7126	3.32	2	5.8634	194.65	-21.71	y	eb
219421171	8.3023	7.89e+03	3.44e+02	9.05e+01	6245	3.57	2	16.753	79.82	-49.64	y	eb
146344020	2.4945	7.88e+03	7.28e+02	2.91e+01	5986	3.94	2	2.5643	74.34	-20.96	n	eb
281053777	11.019	7.86e+03	3.55e+04	2.24e+02	6927	—	1	126.47	98.82	4.19	y	eb
409942986	0.2796	7.81e+03	2.22e+05	6.20e+00	5528	4.22	1	6.2729	145.00	-17.16	n	usp
115693377	4.9269	7.67e+03	4.57e+02	6.05e+01	6136	4.13	2	3.7075	6.81	-41.57	n	eb
460820330	5.0743	7.65e+03	4.49e+02	5.51e+01	6114	4.35	2	38.855	219.39	-31.63	y	eb
270648838	7.6347	7.56e+03	3.17e+04	1.58e+02	6093	4.14	2	50.901	136.70	5.46	y	eb
140212820	0.7777	7.55e+03	1.34e+03	1.58e+01	6392	3.94	2	2.1021	84.96	-30.76	y	eb
270348090	2.8190	7.55e+03	4.59e+02	4.96e+01	—	—	1	20.399	215.48	-30.84	y	eb
269342892	0.2244	7.52e+03	1.31e+04	6.97e+00	—	—	1	0.5568	119.07	-48.24	n	usp
82580956	0.9471	7.48e+03	1.95e+03	2.28e+01	5793	3.93	1	0.4057	169.62	-53.71	y	pl
255548311	4.9631	7.45e+03	2.55e+02	5.80e+01	—	—	1	3.5553	95.48	-50.92	n	eb
146559012	2.6411	7.43e+03	3.54e+04	8.64e+01	6216	4.39	1	17.012	77.51	-23.67	y	eb

Table 1: *Parameters for all 377 WOIs (grouped by classification and in descending order by  $\zeta_{\text{peak}}$ .)*

TIC ID	$P$ [d]	$\zeta_{\text{peak}}$	$\Delta\chi^2$	$\kappa$	$T_{\text{eff}}$ [K]	$\log g$	dips	$\delta$ [%]	RA	Dec	Flat baseline	Class
92628706	9.2030	7.42e+03	1.08e+05	2.30e+02	5547	4.20	1	30.235	315.74	-32.58	y	eb
107012110	3.0334	7.34e+03	5.32e+02	5.40e+01	5994	4.14	1	1.4840	162.04	-40.00	n	pl
451211626	2.4527	7.04e+03	6.29e+02	3.24e+01	3773	4.63	2	41.088	210.31	-34.96	y	eb
279537689	5.7846	7.01e+03	5.36e+02	8.19e+01	5958	4.26	2	3.9806	59.40	-14.16	y	eb
9172417	0.2451	6.89e+03	3.80e+05	5.19e+00	3551	4.67	2	6.4761	62.05	-5.75	n	usp
405391996	1.2851	6.79e+03	1.38e+03	2.06e+01	5764	—	2	1.7041	128.78	-13.75	n	eb
80025900	4.0594	6.71e+03	6.28e+02	6.11e+01	3876	—	2	8.6198	121.00	-46.33	y	eb
231972938	1.5507	6.69e+03	5.75e+02	2.75e+01	6210	4.35	1	3.9200	95.47	-46.21	y	eb
142677613	3.0912	6.64e+03	9.24e+02	5.28e+01	8357	4.16	2	16.442	103.60	-14.45	y	eb
98064760	9.9000	6.60e+03	4.87e+02	7.64e+01	—	—	1	6.7401	289.91	-40.81	y	eb
292293385	0.2694	6.50e+03	3.42e+04	5.26e+00	5492	4.48	1	3.3371	278.49	-69.86	n	usp
167795859	3.1061	6.50e+03	2.75e+02	4.98e+01	5479	4.00	1	16.795	104.42	-61.75	y	eb
387463207	0.1899	6.48e+03	9.64e+06	5.63e+00	6259	4.21	1	27.263	42.46	8.93	n	usp
437230910	0.3805	6.39e+03	3.01e+03	1.48e+01	5406	4.10	1	0.2367	164.77	-21.70	y	pl
396934949	0.1887	6.36e+03	1.74e+04	6.15e+00	4340	4.29	1	4.5204	63.47	3.31	n	usp
96106862	5.3800	6.32e+03	6.05e+02	5.80e+01	6554	4.03	2	1.2424	147.20	-8.49	n	eb
146601318	0.4935	6.27e+03	1.21e+03	1.39e+01	5257	3.75	1	1.9066	149.25	-1.35	y	pl
456609929	4.5678	6.23e+03	1.15e+04	1.59e+01	7643	4.09	2	5.5403	282.35	-59.42	y	eb
130942594	10.792	6.23e+03	1.09e+03	1.32e+02	6362	—	1	20.078	188.34	-32.74	y	eb
87260967	0.5452	6.22e+03	7.45e+03	1.40e+01	4665	—	1	0.1441	272.76	-47.51	y	pl
303811839	6.9220	6.18e+03	4.12e+02	7.14e+01	5938	—	1	2.0336	164.54	-55.98	n	eb
220402290	0.7852	6.12e+03	2.36e+03	1.53e+01	5817	4.36	2	4.5066	69.57	-57.20	n	eb
271225404	2.1195	6.11e+03	5.67e+02	3.20e+01	3764	4.62	2	47.344	211.10	-31.31	y	eb
381948745	1.5953	6.02e+03	4.78e+03	1.37e+01	7084	3.55	1	7.1065	76.36	-56.30	n	eb
128679896	11.130	5.99e+03	8.56e+04	2.35e+02	5594	4.20	2	19.882	299.25	-43.61	y	eb
394657952	0.8723	5.94e+03	1.77e+03	2.02e+01	5725	—	1	2.7255	158.68	-77.96	y	eb
105706808	0.1986	5.93e+03	8.48e+03	7.58e+00	—	—	1	0.4872	156.25	-39.51	n	usp
231840927	1.6357	5.87e+03	1.46e+03	2.17e+01	5726	4.44	2	0.4241	25.17	-65.41	y	eb
231833061	23.335	5.85e+03	1.17e+04	2.31e+02	4580	4.34	2	48.949	24.00	-65.69	y	eb
294328887	0.3545	5.79e+03	1.89e+03	8.30e+00	3079	4.85	1	10.246	108.97	-59.34	n	eb
124712820	0.8256	5.72e+03	1.08e+03	1.69e+01	3989	4.34	2	1.2622	104.76	-11.72	n	eb
312907176	0.7580	5.71e+03	1.21e+03	1.47e+01	3260	5.00	1	43.759	182.91	-68.82	y	eb
307033218	25.755	5.66e+03	1.92e+02	7.51e+01	5216	4.08	1	42.014	123.30	-69.32	y	eb
438682877	0.9221	5.41e+03	1.65e+03	1.56e+01	5820	—	2	0.7677	202.22	-44.68	n	eb
59038880	0.3053	5.29e+03	8.22e+07	4.70e+00	5325	4.62	2	79.385	57.36	12.90	n	eb
412942849	0.3806	5.18e+03	6.39e+03	8.75e+00	6222	3.43	1	0.5721	204.57	-55.57	n	pl
168697816	0.6920	5.17e+03	1.91e+03	1.13e+01	6456	4.37	2	2.4111	61.66	-34.96	n	eb
266816672	0.3031	5.03e+03	7.30e+06	4.92e+00	6064	4.32	2	21.483	30.93	-19.88	n	eb
75818403	0.5635	4.94e+03	7.18e+03	6.93e+00	3669	4.75	2	62.353	139.52	-46.08	n	eb
302038263	1.5474	4.93e+03	8.26e+02	1.96e+01	—	—	2	6.0819	131.95	-69.39	n	eb
23328912	2.5639	4.83e+03	7.65e+02	3.80e+01	8690	4.15	2	0.8293	167.44	-35.40	n	eb
1190662	0.4440	4.79e+03	1.30e+03	1.76e+01	3595	4.28	2	2.3930	136.03	-16.49	y	eb
125501325	4.3858	4.77e+03	7.40e+02	4.11e+01	—	—	2	5.9093	105.85	-10.70	n	eb
13738984	0.2769	4.76e+03	1.69e+04	6.68e+00	5818	4.35	2	0.5887	133.70	-11.03	n	usp
89787749	0.5413	4.75e+03	6.98e+02	1.68e+01	3374	4.91	1	23.436	127.87	-59.20	n	eb
92938279	0.2750	4.66e+03	2.92e+05	4.38e+00	3327	4.89	2	18.534	83.63	-22.64	n	usp
92938280	0.2750	4.54e+03	1.20e+05	4.45e+00	3396	4.95	2	15.406	83.63	-22.64	n	usp
29847695	4.9980	4.46e+03	7.29e+02	5.01e+01	6375	—	2	7.6000	23.58	-8.45	y	eb
350740905	0.1555	4.37e+03	1.88e+05	4.22e+00	8181	3.86	1	0.8493	88.55	-56.17	n	usp
436243444	0.6793	4.33e+03	9.70e+02	1.70e+01	5093	4.24	1	3.2989	84.13	8.43	y	eb
396953669	0.3327	4.30e+03	7.56e+03	6.55e+00	4719	—	2	0.3230	63.88	3.36	n	eb
30287190	3.1243	4.21e+03	3.17e+02	4.35e+01	6217	4.16	2	2.6468	207.60	-31.23	n	eb
2353789	1.8718	4.20e+03	8.55e+02	1.98e+01	6969	3.91	1	3.0641	134.27	-28.77	n	eb
279454212	11.762	4.17e+03	2.06e+02	7.62e+01	5951	4.42	1	4.1042	58.47	-16.95	y	eb
425206178	0.1647	4.07e+03	1.41e+04	4.97e+00	—	—	1	6.2160	111.55	7.68	n	usp
161570793	0.2762	4.04e+03	4.21e+05	4.29e+00	6262	4.37	2	4.9210	74.44	-42.89	n	usp

Table 1: Parameters for all 377 WOIs (grouped by classification and in descending order by  $\zeta_{\text{peak}}$ .)

TIC ID	$P$ [d]	$\zeta_{\text{peak}}$	$\Delta\chi^2$	$\kappa$	$T_{\text{eff}}$ [K]	$\log g$	dips	$\delta$ [%]	RA	Dec	Flat baseline	Class
269762258	1.3247	3.99e+03	4.10e+04	2.63e+01	3358	4.67	2	11.874	66.47	-81.31	y	eb
20095466	0.2118	3.97e+03	2.75e+03	7.97e+00	5966	4.49	1	0.2755	89.22	-36.07	y	usp
284729177	0.2068	3.88e+03	6.91e+04	4.44e+00	7571	3.43	1	1.4845	67.66	10.60	n	usp
185805011	2.0054	3.78e+03	7.87e+02	1.85e+01	3477	4.83	2	27.171	130.69	-31.03	y	eb
214299966	3.0675	3.64e+03	5.70e+02	3.30e+01	6181	4.14	1	1.7140	339.16	-36.94	n	pl
147102369	2.0638	3.46e+03	4.47e+02	3.45e+01	7231	3.84	2	5.8315	124.80	-30.42	y	eb
381854774	1.6447	3.45e+03	7.77e+02	2.21e+01	6375	4.12	1	1.0266	321.79	-54.34	y	pl
178889597	1.8842	3.43e+03	7.90e+02	2.99e+01	4777	—	1	2.4647	195.12	-38.84	y	eb
282051803	2.4625	3.41e+03	1.00e+03	2.24e+01	6246	3.87	2	7.0610	132.22	-75.92	y	eb
186544053	8.9117	3.41e+03	2.15e+02	4.64e+01	—	4.67	1	1.7649	132.92	-33.10	y	pl
198008281	0.2631	3.36e+03	3.04e+06	4.21e+00	7089	4.04	2	3.2852	60.26	-54.40	n	usp
33689349	3.4974	3.25e+03	6.85e+02	2.50e+01	7098	4.10	2	24.721	92.93	-17.68	y	eb
406276109	7.5474	3.23e+03	3.26e+02	4.51e+01	3200	4.82	2	10.415	325.64	-64.21	n	eb
243391171	1.5167	3.18e+03	4.65e+03	1.52e+01	5943	—	1	2.3712	205.06	-45.70	n	eb
335452175	7.7501	3.16e+03	4.01e+03	6.51e+01	—	—	1	0.8537	226.27	-47.05	n	pl
360571125	2.4626	3.13e+03	7.99e+02	2.53e+01	9517	3.60	2	1.1710	263.87	-55.76	y	eb
167007869	0.5509	3.10e+03	2.12e+03	1.06e+01	4949	—	1	0.1814	94.80	-67.59	n	misc
9433212	5.0138	3.07e+03	1.45e+02	3.70e+01	5878	4.17	2	4.2410	73.54	-9.49	n	eb
403136932	0.3028	3.05e+03	4.15e+05	3.93e+00	3391	4.82	2	46.579	333.76	-54.27	n	eb
332003916	0.6461	3.02e+03	1.71e+04	5.50e+00	7458	3.54	4	0.7006	179.10	-48.79	n	misc
349523518	0.1977	3.02e+03	2.61e+04	3.93e+00	6172	4.07	1	3.6427	111.49	-63.22	n	usp
277912443	0.5379	3.01e+03	2.10e+03	9.50e+00	5964	4.04	1	0.6526	354.44	-73.91	n	misc
129781743	0.2012	3.01e+03	9.79e+03	5.36e+00	6655	4.24	1	0.7832	36.24	-38.68	n	usp
350518984	10.367	3.00e+03	1.40e+02	6.01e+01	7029	—	1	2.8731	86.18	-56.71	y	eb
72229825	1.7954	2.99e+03	1.78e+02	2.11e+01	6415	4.41	1	1.5651	186.75	-43.67	n	pl
350479101	5.9589	2.98e+03	2.65e+02	5.77e+01	6662	4.05	1	2.7658	85.79	-59.14	y	eb
272086869	3.9823	2.97e+03	3.02e+02	3.20e+01	8799	4.03	2	1.7775	115.67	-72.53	y	eb
349154435	4.4313	2.96e+03	2.13e+02	3.36e+01	5832	4.19	2	4.1264	108.18	-62.01	y	eb
349911034	0.5385	2.92e+03	9.12e+02	1.17e+01	5799	4.20	1	1.6651	113.97	-65.68	y	pl
270427198	2.5609	2.85e+03	2.07e+04	4.40e+00	6984	3.35	3	0.7279	96.35	-78.57	n	misc
255567460	6.8989	2.84e+03	2.13e+02	4.38e+01	9984	4.35	1	1.3900	96.44	-53.10	y	pl
312068854	7.1007	2.82e+03	1.38e+02	5.83e+01	5716	4.31	1	1.5401	140.02	8.44	y	pl
52382500	0.1968	2.80e+03	5.32e+04	3.97e+00	5944	3.61	1	1.7025	24.19	-69.95	n	usp
48318875	0.3028	2.76e+03	7.34e+04	4.24e+00	5873	3.99	2	4.2039	223.30	-31.62	n	eb
24347173	0.3516	2.75e+03	1.57e+03	1.16e+01	5744	4.22	2	0.8472	79.17	-8.70	n	eb
289596375	7.2587	2.72e+03	4.74e+02	4.22e+01	6170	3.59	2	2.7868	131.79	-13.06	y	eb
92743594	8.4461	2.70e+03	2.92e+02	3.26e+01	4835	—	4	1.9285	129.00	-53.61	y	eb
453828066	9.1358	2.67e+03	4.58e+02	4.04e+01	6545	4.08	1	9.3237	53.36	0.11	n	eb
166319733	0.1410	2.66e+03	5.82e+04	4.09e+00	5425	3.86	1	5.0870	206.68	-37.76	n	usp
372909935	3.6118	2.64e+03	2.09e+02	3.64e+01	7015	4.12	1	1.1117	119.45	-64.21	y	pl
244252435	0.9435	2.62e+03	2.45e+04	3.39e+01	3675	4.57	2	5.4926	74.37	-3.95	n	eb
23555025	4.7455	2.62e+03	2.34e+02	3.59e+01	6001	4.34	1	4.1329	169.03	-32.65	n	eb
362086333	0.2828	2.61e+03	9.33e+03	5.41e+00	10440	4.18	1	1.0040	107.90	-84.46	n	usp

This paper has been typeset from a  $\text{\LaTeX}$  file prepared by the author.